Different Er3+ environments in Mg-based nanoparticles-doped optical fibre preforms

Francesco d'Acapito, Wilfried Blanc, Bernard Dussardier

Different Er^{3+} environments in Mg-based nanoparticles-doped optical fibre preforms

F. d'Acapito[a], W. Blanc[b,*], B. Dussardier[b]

[a] *CNR-IOM-OGG Grenoble*
[b] *Univ. Nice Sophia Antipolis, CNRS, LPMC, UMR7336, 06100 Nice, France*

Abstract

Developing new rare-earth ions-doped optical fibres for power amplifiers and lasers requires continuous improvements in fibres spectroscopic properties. To overcome some limitations inherent to silica glass, it is proposed to embed rare-earth ions in dielectric nanoparticles. In this article we focus on the modifications of the Er^{3+} ions spectroscopy in Mg-silicate nanoparticles doped into optical fiber preforms. Through EXAFS and fluorescence measurements, we demonstrate that different local environments are experienced by Er^{3+} ions, attributed to the depolymerization of the phosphate network. These results gain insight into the tayloring of luminescence properties.

Keywords: silica, erbium, nanoparticles, magnesium, EXAFS, fluorescence, optical fiber

1. Introduction

Developing new rare-earth ions (RE)-doped optical fibres for power amplifiers and lasers requires continuous improvements in the fibres spectroscopic properties besides reduction in device size and economical efficiency. However, some potential applications of RE-doped fibres suffer from limitations in terms of spectroscopic properties resulting from RE clustering or inappropriate local environment when they are inserted into silica. An interesting solution consists in using silica as a mechanical host and support of the fibre optical waveguide, and in embedding RE-ions within nanoparticles (NP) of appropriate composition and structure [1, 2, 3].

The original route proposed by LPMC to obtain NP in fibres is based on the industrial MCVD (Modified Chemical Vapor Deposition) process. As silicate systems have a strong stable immiscibility when they contain divalent metal oxides, we take advantage of thermal treatments inherent to this process to obtain NP through the phase separation mechanism. Through this route, NP are grown in-situ within the material when alkaline-earth ions (Mg, Ca and Sr) are incorporated into the fibre core [4, 5, 6]. In particular cases the effect of the divalent metal is also to prevent the clustering of Er^{3+} in phosphate phases as shown for similar samples in [7]. In these samples, the spectroscopic behaviour of Er^{3+} ions depends on the concentration of the alkaline-earth ions [8]. To explain these modifications, we study, in this article, the local order around Er^{3+} by Extended X-ray Absorption Spectroscopy (EXAFS) which permits to cast a link between local geometry and optical response. EXAFS at the $Er - L_{III}$ edge has already revealed to be effective in the description of the site of Er^{3+} [7] and Yb^{3+} [2] in optical fibre preforms with nanoparticles obtained by phase separation. It revealed a marked affinity between the RE and phosphate phases.

2. Experimental

2.1. Sample preparation

Preforms were fabricated by the conventional MVCD technique [9]. The so-called 'solution doping technique' [10] was applied to incorporate magnesium and erbium ions: the core porous layer, doped with GeO_2 and P_2O_5, is soaked with an alcoholic solution of $ErCl_3 : 6H_2O$ and $MgCl_2 : 6H_2O$ of desired concentrations. After drying of the solvent, the core layer is sintered down to a dense glass layer. Then the tube is collapsed into a solid rod, referred to as preform, at an elevated temperature higher than 1800 °C. Preforms are stretched into 125-μm fibres using a drawing tower at

*Corresponding author. Tel.: +33-492-076-799; Fax.: +33-492-076-754

Email address: wilfried.blanc@unice.fr (W. Blanc)

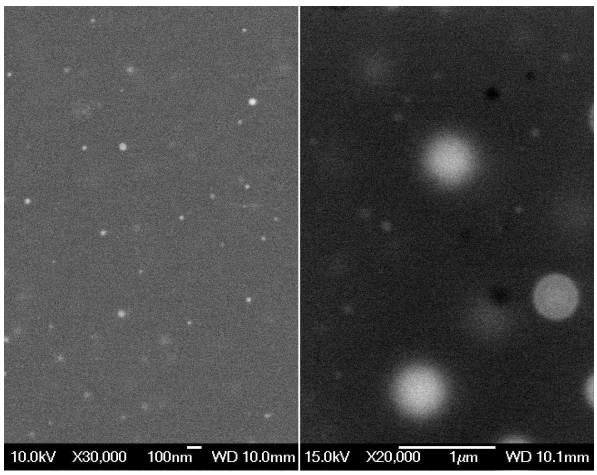

Figure 1: SEM pictures of Mg-0.1 (left) and Mg-1.5 (right) preforms.

temperatures higher than 2000 °C under otherwise normal conditions. Here we report on samples labeled as Mg-X doped with solutions containing X=0, 0.1, 0.3, 0.5, 0.7, 1 and 1.5 mol/l of $MgCl_2$ salts. To investigate the role of phosphorus, two samples were prepared without this element and are labeled Mg-XnoP. Preform compositions were estimated from Energy Dispersive X-Ray measurements ($160 \times 130 \mu m^2$ scanned area in the core) and Electron Probe Microanalyses. It was found that GeO_2 and P_2O_5 mean concentrations are 0.8 mol% and 0.4 mol%, respectively. MgO concentration increases from 0.1 (Mg-0.1) to 5.5 mol% (Mg-1.5). Doping with Mg leads to the formation of nanoparticles in the core. SEM pictures for the Mg-0.1 and Mg-1.5 samples are presented in Fig.1. As previously observed, the mean size of the nanoparticles increases with Mg concentration [8]. It is about 50 nm in Mg-0.1 up to hundreds of nm in Mg-1.5. Optical losses induced by the NP have been discussed in a previous paper [8]. The erbium concentration of 0.01 mol/l was kept constant in the doping solution and the erbium ion concentration in samples was previously estimated to be 200 ppm [8].

2.2. Photoluminescence

Emission spectra of Mg-doped core of the preforms were recorded at room temperature. The beam from a continuous 980 nm, 250-mW fiber-coupled laser diode was coupled into the tested preform through a single-mode fiber-coupler. The 1550 nm fluorescence was collected from the second coupler arm and it was directed, through an isolator, to an optical spectrum analyzer (Anritsu MS9701C). The resolution of the OSA was 1 nm. Emission spectra reported in Fig.2 are averaged on twenty sweeps and the signal is smoothed on

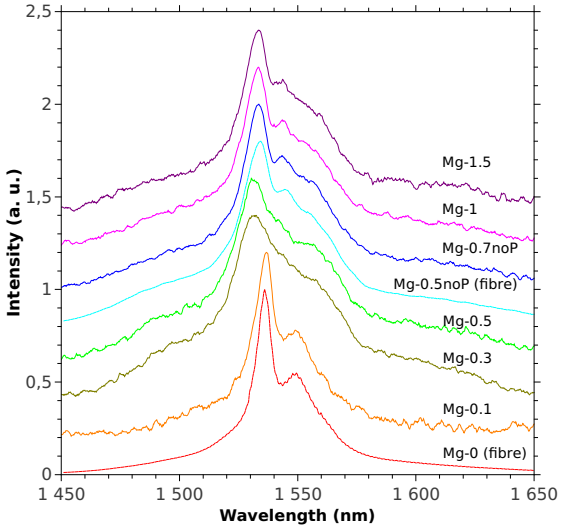

Figure 2: Emission spectra of Mg-doped preforms (continuous lines) and fibres (dashed lines) recorded at room temperature. Excitation wavelength is 980 nm. Each spectrum is shifted vertically by 0.2.

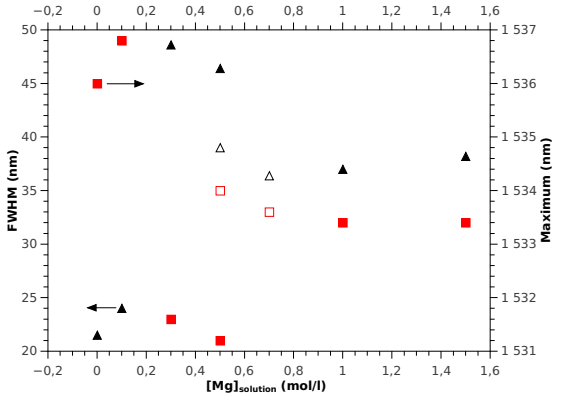

Figure 3: FWHM (triangles) and wavelength of the maximum of fluorescence intensity (squares) *vs* Mg concentration. Open symbols are related to the samples without P.

eleven points. FWHM and wavelength of the maximum of fluorescence intensity are reported in Fig.3.

2.3. X-ray Absorption Spectroscopy

XAS measurements have been carried out at the GILDA-CRG beamline BM08 at the European Synchrotron Radiation Facility [11]. The monochromator was equipped with a pair of Si(311) crystals and was run in dynamical (horizontal) focusing mode [12]. The harmonic rejection as well as the vertical focusing was achieved by using a pair of Pd-coated mirrors with a cut-off energy $E_{cutoff} = 18\,keV$. This optical arrangement permitted to obtain a focal spot of about $200\times200\,\mu m$ on the sample location, small enough to probe the core of the preform. The absorption coefficient was measured in fluorescence mode by using an energy resolving detector (12-elements array High Purity Ge). The spectra are shown in Fig.4 whereas the related Fourier Transforms are shown in Fig.5.

The structural model used for the quantitative data analysis is the same used in previous literature for this class of systems [13, 14, 15]: a RE ion linked to a SiO_4 tetradedron with a well defined Er-O distance and Er-O-Si bond angle. Here we note that, due to the similar backscattering amplitude and phase of Si, P and Mg it is not possible to distinguish these three atoms in the second coordination shell. The data analysis was carried out with the ATHENA and ARTEMIS [16] codes and the theoretical XAS paths were generated with the Feff8.10 code [17] starting from the $Er_2Si_2O_7$ crystal structure [18]. The EXAFS signal was modelized by using the main scattering signals originating from the Er-O-Si triangular configuration as thoroughly discussed in [14]. The Debye Waller factor of the second shell was fixed to 0.002 Å^2 whereas the number of oxygen first neighbors was linked to the Er-O bond length by using the data from the Bond Valence Method (BVM, [19]). BVM has been suggested in literature as an effective method in XAS data analysis to reduce the correlation between fit parameters [20]. By using the parameters published in [21] the relationship between the number of O atoms N_O and the Er-O bond length R_{Er-O} can be approximated as :

$$N_O \approx 63.343 - 67.499 \times R_{Er-O} + 18.695 \times R^2_{Er-O}$$

The results of the quantitative analysis are shown in Table1.

3. Results and Discussion

From Fig.2 and Fig.3, Er^{3+} fluorescence properties can be separated into three Mg-concentration domains.

Sample	N_O	R_{Er-O} (Å)	σ^2_O (Å^2)	R_{Er-Si} (Å)
Mg-0	4	2.30(2)	0.01(5)	-
	4	2.37(2)	0.01(5)	-
Mg-0.1	7(1)	2.31(6)	0.013(6)	3.7(2)
Mg-0.3	6.9(7)	2.30(4)	0.013(4)	3.7(1)
Mg-0.5	6.9(7)	2.29(4)	0.011(4)	3.7(1)
Mg-0.5noP	6(1)	2.24(3)	0.006(1)	3.6(1)
Mg-0.7noP	7(1)	2.28(6)	0.014(6)	3.6(2)
Mg-1	6.3(7)	2.26(4)	0.012(4)	3.6(1)
Mg-1.5	6.2(7)	2.26(4)	0.012(4)	3.6(1)

Table 1: Results of the quantitative analysis of the EXAFS data. Sample Mg-0 is fitted with a crystalline $ErPO_4$ model.

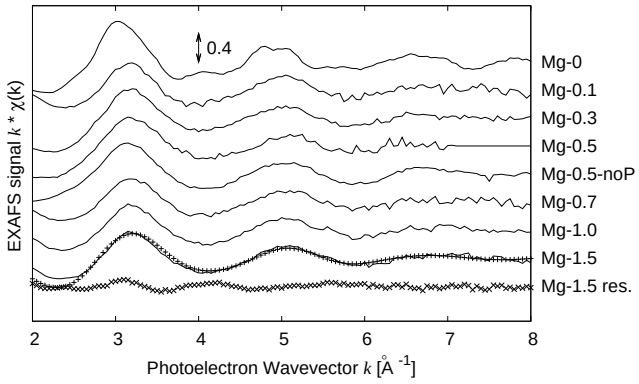

Figure 4: EXAFS spectra of the various Mg-doped samples (0.1-1.5) compared with a sample without divalent codopant (Mg-0). For Mg-1.5 also the fit is shown (+) with the residual (×).

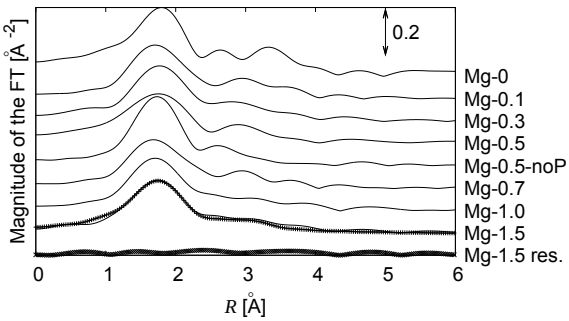

Figure 5: Fourier Transforms of the spectra shown in Fig.4. For Mg-1.5 also the fit is shown (+) with the residual (×).

At low concentration (Mg-0 and Mg-0.1), FWHM is about 20-25 nm and the main peak position is at 1536 nm. These values correspond to those measured in a P-doped silica fiber [22]. For intermediate Mg concentration (Mg-0.3 and Mg-0.5), FWHM increases up to 45-50 nm, the peak position shifts to shorter wavelengths and the spectrum appears poorly structured. As particle sizes increase compare to previous samples, one may expect that the fluorescence spectrum could be influenced by reabsorption effect. However, this effect would shift peak position to longer wavelengths. For the highest Mg concentration (Mg-1 and Mg-1.5), FWHM and peak position values are 35-40 nm and 1533 nm, respectively, whereas structures appear in the long wavelength side of the line. These two values are close to those reported for samples without P (open symbols in Fig.3). They can also be compared with values reported for alumino-germano-silicate fibre (type II in [22]): FWHM and peak position are 40 nm and 1533 nm, respectively.

The EXAFS spectra (Fig.4) show less differences respect to optical fluorescence with the exception of Mg-0 sample which contains more oscillating components than the others as also confirmed by the Fourier Transform (FT) (Fig.5). As previously reported for this sample [7], the additional signals above the first coordination shells are due to the formation of nuclei with the $ErPO_4$ structure. This P-cage effect has been already reported [23]. However, the fluorescence spectrum of Mg-0 does not present any features of crystalline phase [24] suggesting that this phase is not spatially extended and consist of only a few coordination shells (around 4-5 Å). The Mg-doped samples exhibit a dominant oscillation due to a Er-O coordination shell (Fig. 4). The FT confirms this idea as it shows only a dominant main peak at about 1.8 Å (Fig. 5). This situation is typical of rare-earth ions embedded in a glassy matrix. By increasing Mg concentration, R_{Er-O} smoothly decreases from 2.31 down to 2.26 Å and the resulting N_0 decreases from 7 to 6 (Table 1).

Both fluorescence and EXAFS measurements demonstrate that Er^{3+} ions experience different environements with Mg concentration. In the Mg-0 sample, a well organised solvation shell is formed by P around Er as already observed with this RE [23, 24] and Yb [2]. In the Mg-doped samples, the composition of the environment can not be determined exactly from EXAFS measurements as Mg, Si and P can not be distinguished with EXAFS analyses. However, we have reported that, in Mg-doped samples, Er ions are located in the nanoparticles which contain also P and Mg ions [25]. Concentrations of these three elements in the NP are expected to be higher than the mean concentrations reported in 2.1. Then, Mg-0.3 and Mg-0.5 results could be explained by assuming a P-rich and/or well polymerized environment. Indeed, the degree of glass polymerization has been found to be correlated to the RE-O bond length in phosphate glasses [26]. In the case of ultraphosphate glasses, N_0=7.3 and R_{Er-O}=2.29 Å have been reported by [26], in accordance with Mg-intermediate concentration results. Moreover, FWHM of Er^{3+} emission bands in phosphate glasses is usually larger compare to those reported in silicate [27]. When Mg concentration increases, phosphate network tends to depolymerize [28, 29]. In the less polymerized metaphosphate glass, N_0=6.3 and R_{Er-O}=2.23 Å [26], as observed for the highest Mg concentration. FWHM tends also to decrease when Mg is added to a phosphate glass [30]. However, for the highest Mg concentrations, the presence of P in the local environment of Er can not be asserted from these measurements as same characteristics are obtained in P-doped samples (Mg-1 and Mg-1.5) and P-free samples (Mg-0.5noP and Mg-0.7noP).

4. Conclusion

In this article we report on the modification of the erbium ions environment by changing Mg concentration. Different environments are identified by comparing fluorescence and EXAFS measurements. These changes are attributed to the depolymerization of the phosphate network. These results gain insight into the tayloring of luminescence properties of RE-doped optical fibres.

Acknowledgements

Authors greatly acknowledge Michèle Ude and Stanislaw Trzesien (LPMC) for the preparation of the preforms, Olivier Tottereau (Univ. Nice Sophia Antipolis, CNRS, CRHEA, UPR 10, Valbonne, France) for SEM/EDX measurements and Ivan Kasik for EPMA measurements realized at the Institute of Photonics and Electronics of the Academy of Sciences of the Czech Republic. GILDA is a project jointly financed by CNR and INFN.

References

[1] B. Samson, P. Tick, N. Borrelli, Optics letters 26 (2001) 145–147.

[2] C. Oppo, R. Corpino, P. Ricci, M. Paul, S. Das, M. Pal, S. Bhadra, S. Yoo, M. Kalita, A. Boyland, J. Sahu, P. Ghigna, F. dAcapito, Optical Materials 34 (2012) 660 – 664.

[3] J. Thomas, M. Myara, L. Troussellier, E. Burov, A. Pastouret, D. Boivin, G. Mélin, O. Gilard, M. Sotom, P. Signoret, Optics express 20 (2012) 2435–2444.
[4] W. Blanc, B. Dussardier, G. Monnom, R. Peretti, A.-M. Jurdyc, B. Jacquier, M. Foret, A. Roberts, Appl. Opt. 48 (2009) G119–G124.
[5] W. Blanc, B. Dussardier, M. C. Paul, Glass Technology - European Journal of Glass Science and Technology Part A 50 (2009) 79–81.
[6] W. Blanc, V. Mauroy, B. Dussardier, Int. J. of Nanotechnology 9 (2012) 480–487.
[7] F. dAcapito, C. Maurizio, M. Paul, T. S. Lee, W. Blanc, B. Dussardier, Materials Science and Engineering: B 146 (2008) 167 – 170.
[8] W. Blanc, V. Mauroy, L. Nguyen, B. Shivakiran Bhaktha, P. Sebbah, B. P. Pal, B. Dussardier, Journal of the American Ceramic Society 94 (2011) 2315–2318.
[9] H. P. J.B. Mac Chesney, P.B. Oapos Connor, Proc IEEE 62 (1974) 1280–1281.
[10] S. P. J.E. Townsend, D. Payne, Elect. Lett. 23 (1987) 329–331.
[11] F. D'Acapito, S. Colonna, S. Pascarelli, G. Antonioli, A. Balerna, A. Bazzini, F. Boscherini, F. Campolungo, G. Chini, G. Dalba, I. Davoli, P. Fornasini, R. Graziola, G. Licheri, C. Meneghini, F. Rocca, L. Sangiorgio, V. Sciarra, V. Tullio, S. Mobilio, ESRF Newsletter 30 (1998) 42.
[12] S. Pascarelli, F. Boscherini, F. D'Acapito, J. Hrdy, C. Meneghini, S. Mobilio, J. Synchrotron Rad. 3 (1996) 147.
[13] F. D'Acapito, S. Mobilio, P. Gastaldo, D. Barbier, L. F. Santos, O. Martins, R. M. Almeida, J. Non-Cryst. Solids 293-295 (2001) 118–124.
[14] F. D'Acapito, S. Mobilio, S. Scalese, A. Terrasi, G. Franzò, F. Priolo, Phys. Rev. B 69 (2004) 153310.
[15] F. D'Acapito, S. Mobilio, P. Bruno, D. Barbier, J. Philipsen, J. Appl. Phys. 90 (2001) 265.
[16] B. Ravel, M. Newville, J. Synchrotron Rad. 12 (2005) 537–541.
[17] J. J. Rehr, R. C. Albers, Rev. Mod. Phys. 72 (2000) 621–654.
[18] Y. Smolin, Y. Shepelev, Acta Crystall. B 26 (1970) 484.
[19] I. D. Brown, D. Altermatt, Acta Crystallographica Section B 41 (1985) 244–247.
[20] M. Newville, Physica Scripta 2005 (2005) 159.
[21] I. D. Brown, 2011. Http://www.iucr.org/resources/data/datasets/bond-valence-parameters.
[22] E. Desurvire, Erbium-doped fiber amplifiers: Principles and applications, Wiley (New York), 1994.
[23] A. Saitoh, S. Matsuishi, C. Se-Weon, J. Nishii, M. Oto, M. Hirano, H. Hosono, J. Phys. Chem. B 110 (2006) 7617–7620.
[24] R. Peretti, A. Jurdyc, B. Jacquier, W. Blanc, B. Dussardier, Optical Materials 33 (2011) 835–838.
[25] W. Blanc, C. Guillermier, B. Dussardier, Opt. Mater. Express 2 (2012) 1504–1510.
[26] M. Karabulut, E. Metwalli, A. Wittenauer, R. Brow, G. Marasinghe, C. Booth, J. Bucher, D. Shuh, Journal of Non-Crystalline Solids 351 (2005) 795 – 801.
[27] S. Jiang, M. Myers, N. Peyghambarian, Journal of Non-Crystalline Solids 239 (1998) 143 – 148.
[28] G. Walter, U. Hoppe, T. Baade, R. Kranold, D. Stachel, Journal of non-crystalline solids 217 (1997) 299–307.
[29] I. Wacławska, M. Szumera, Journal of thermal analysis and calorimetry 84 (2006) 185–190.
[30] S. Jiang, T. Luo, B.-C. Hwang, F. Smekatala, K. Seneschal, J. Lucas, N. Peyghambarian, Journal of Non-Crystalline Solids 263264 (2000) 364–368.